JOURNAL OF CATALYSIS **166,** 294–305 (1997)
ARTICLE NO. CA971522

Structural Characterization of Rhodium-Containing Hydrodesulfurization (HDS) Catalysts Derived from a Laser Vaporization Cluster Source[1]

James R. Brenner, Christopher L. Marshall,[2] George C. Nieman,[3] Eric K. Parks, Stephen J. Riley, Leroy Ellis,[4] Nancy A. Tomczyk, and Randall E. Winans

Chemistry Division, Argonne National Laboratory, 9700 South Cass Avenue, Argonne, Illinois 60439-4831

Received June 21, 1996; revised November 6, 1996; accepted November 7, 1996

A series of highly dispersed Rh-based materials have been prepared by deposition of laser-generated gas-phase clusters onto an industrial-grade alumina. While the diameter of the gas-phase metal clusters could be kept at or below 1 nm, the average diameter of the resulting supported Rh particles was always at least 1.5 nm. The reaction of the clusters with either O_2 or C_2H_4 failed to prevent Rh aggregation on the alumina surface. The addition of O_2 upstream of the Rh target was sufficient to form bulk Rh_2O_3, whereas downstream addition of O_2 or C_2H_4 to the Rh clusters was insufficient to form Rh oxide particles. Most of the Rh-containing particles further aggregated during either sulfiding or HDS testing. Nevertheless, the resulting rhodium sulfides were comparable in activity to sulfided, commercial Co–Mo or Ni–Mo catalysts on a per gram of catalyst basis and superior on a per gram of metal basis. At low loadings (0.1 wt%), the cluster-derived catalysts were more hydrogen-efficient than the commercial catalysts. © 1997 Academic Press

INTRODUCTION

Over the past two decades, the study of the physical (1–23), chemical (3, 4, 15, 23–35), electronic (5, 6, 17, 23, 36–48), and magnetic (49–57) behavior of vapor-phase generated, subnanometer metal clusters has been a subject of considerable interest to those in the fields of heterogeneous catalysis and electronics nanofabrication. Metal clusters of $\leq$100 atoms ($\leq$1-nm diameter) are of scientific importance because the aforementioned properties change from predominately molecular to bulk in character as the clusters grow in size (38).

Rhodium is a metal of particular interest to manufacturers of catalysts for automotive exhaust and specialty chemicals applications. However, Rh metal clusters have been largely ignored by the metal cluster community, with the following exceptions. Kaldor and Cox (24) report a suprisingly high H_2 chemisorption on Rh clusters containing one or two Rh atoms (H/Rh = 8) and no chemisorption of CH_4 onto Rh clusters of any size. Freiser (12) reports that alkanes from C_4–C_{10} undergo limited dehydrogenation over Rh^+ ions under electron impact conditions. Bloomfield and coworkers (56–57) claim that Rh clusters exhibit giant magnetic moments.

Laser vaporization has become the method of choice for generating ligand-free metal clusters because it can be used to evaporate even the most refractory metals (42, 58–64). Our laser vaporization cluster source is unique in that the metal of interest is vaporized from a metal target located in a continuous flow of He. The vaporized metal (mostly neutral atoms) is quickly quenched in He carrier gas, and cluster growth occurs chiefly by atom addition, also known as Ostwald ripening (65).

Several groups have deposited metal clusters onto low surface area supports such as single crystals (66), microscope grids (13–15, 66–68), and highly-oriented pyrolitic graphite (69) in order to better characterize the metal clusters. However, work describing the deposition of metal clusters onto high surface area supports have not been reported, and work describing the use of supported, ligand-free metal clusters as catalysts has been rare (15, 70). Such work is critical if a link between the basic science of unsupported metal clusters and applied catalysis is to be established. For clarity, all future references to the term "cluster" will refer to vapor phase metal, and references to the term "particle" will refer to alumina-supported metal.

In this work, we used the laser vaporization method to deposit small Rh metal clusters onto a high surface area alumina and then tested sulfided versions of these alumina-supported Rh particles as hydrodesulfurization (HDS) catalysts in order to assess the following issues:

(1) Is the size of supported metal particles governed by the deposition process or by aggregation phenomena

[1] This article has been authored by a contractor of the U.S. Government under contract No. W-31-109-ENG-38. Accordingly, the U.S. Government retains a nonexclusive, royalty-free license to publish or reproduce the published form of this contribution, or allow others to do so, for U.S. Government purposes.

[2] To whom correspondence should be addressed. E-mail: clmarshall@anl.gov.

[3] Permanent address: Monmouth College, Monmouth, IL.

[4] Permanent address: Arco Exploration and Production Technology, Plano, TX.

0021-9517/97 $25.00

following either deposition, further synthesis steps, or catalysis?

(2) If the size of supported metal particles is governed by aggregation phenomena following deposition, does the addition of reagent gases prevent this aggregation?

(3) What effect does the oxidation state of the metal precursor have on the eventual metal dispersion? Is an oxidized metal precursor necessary to form a strong enough metal–support interaction to keep the metal clusters from migrating across the alumina surface to form larger metal particles?

(4) What impact does metal particle size have on catalytic behavior?

METHODS

Synthesis

Clusters were made by laser vaporization of a Rh target located in a continuous flow of He gas using the apparatus shown in Fig. 1 (63–64). The target was formed from a sheet of unknown purity rolled into a 0.25 inch diameter rod (1 inch = 0.0254 m), with the resulting seam welded using an electron beam. Mass spectrometry of clusters vaporized from the Rh target indicated the presence of a 0.1 wt% Fe + Fe oxide impurity. The vaporized metal (mostly neutral atoms) was quickly quenched by He at 5–75 Torr pressure (1 Torr = 133.3 N m^{-2}). In some cases, O_2 or C_2H_4 was added to the flow stream in an attempt to form an oxide or carbide coating, respectively. The reagent gas could be added either upstream of the Rh target, in which case it is present in the vaporization plasma, or downstream of the Rh target. In most cases, the reagent gas was added near the end of the cluster growth region, although some cluster growth likely occurs subsequent to reagent gas addition. Reaction times were typically 0.1–0.5 ms. Clusters exiting a nozzle at the end of the flow tube were formed into a molecular beam in high vacuum. The expansion out of the nozzle increases the translational energy of the clusters and decreases their internal energy. The translational energies depend on both cluster size and the temperature of the cluster source, which in our system can be varied from −170 to 150°C.

The clusters were transported to a laser-ionization time-of-flight mass spectrometer for cluster size determination. The mass spectrometer is oriented perpendicular to the direction of the cluster beam. After ionization by an ArF excimer laser, the clusters were directed onto an ion detector by deflection plates located within the mass spectrometer. Cluster translational energies were determined by modeling the ion trajectories with a simulation program (MacSimion), using the deflection plate voltages that maximize the ion signal for a particular cluster size. The internal energies of the clusters are more difficult to determine, since the degree of expansion cooling cannot be measured. It is likely that the clusters were somewhat cooler than the cluster source temperature. The conditions used for the metal cluster depositions are summarized in Table 1.

For the collection experiments, a baffled cylindrical basket (Fig. 2) capable of holding up to 2.5 g of alumina support was positioned in front of the molecular beam. This basket was rotated continuously to ensure uniformity of the collected product. The support material was a gamma–alumina synthesized from LaRoche V–GL boehmite by calcining in 1% O_2/He (AGA) at 600°C for 1 h. Following calcination, the alumina had a surface area of 270 m^2/g. The "s" in SR-1s, SR-3s, and SR-7s (Table 1) means that the corresponding

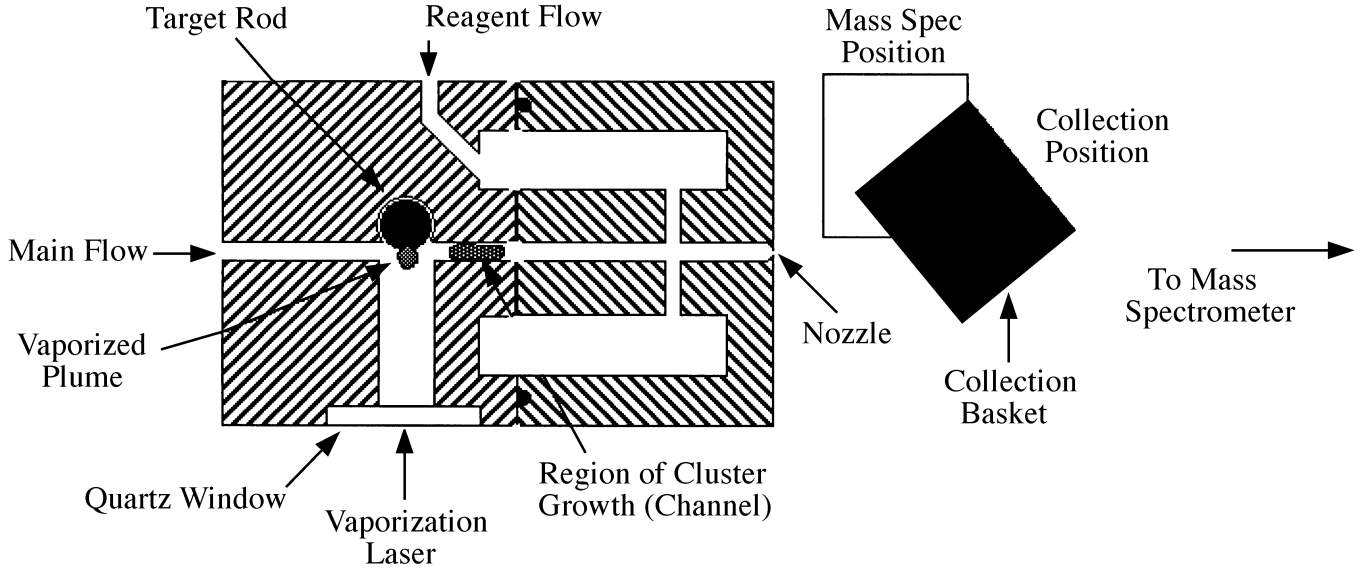

FIG. 1. Schematic of laser vaporization cluster source.

TABLE 1

Preparation of Materials

Code	Composition	Channel length (mm)	Helium pressure (Torr)	Deposition time (h)	Cluster source temperature (°C)	Reagent gas (mTorr)
SR-1	Fresh 0.1% Rh/Al_2O_3	21.1	20.0	1.0	20	None
SR-1s	Spent[a] 0.1% Rh/Al_2O_3	21.1	20.0	1.0	20	None
SR-3	Fresh 0.5% Rh/Al_2O_3	27.5	7.8	3.5	−160	None
SR-3s	Spent[a] 0.5% Rh/Al_2O_3	27.5	7.8	3.5	−160	None
SR-4	Fresh 0.5% RhO_x/Al_2O_3	27.5	7.8	2.3	−160	O_2 (6.9)
SR-5	Fresh 0.5% Rh/Al_2O_3	21.1	7.8	2.5	−160	None
SR-6	Fresh 0.5% Rh/Al_2O_3	21.1	7.8	2.5	−160	C_2H_4 (71.3)
SR-7	Fresh 0.5% Rh/Al_2O_3	27.5	75.0	0.6	20	None
SR-7s	Fresh 0.5% Rh/Al_2O_3	27.5	75.0	0.6	20	None
SR-8	Fresh 0.5% RhO_x/Al_2O_3	21.1	7.8	3.5	−160	O_2 (27)[b]

[a] Spent (or s as in SR-1s) = Sulfided in 5% H_2S/H_2 at 400°C for 2 h, then used for dibenzothiophene hydrodesulfurization.
[b] Oxygen added upstream of the target causes formation of bulk Rh oxide clusters, as opposed to surface coating of oxide for SR-4 and carbide for SR-6.

SR-1, SR-3, and SR-7 have been sulfided and used as a hydrodesulfurization (HDS) catalyst.

Transmission Electron Microscopy

Approximately 0.01 g of cluster/alumina material was placed into a vial containing ~10 ml of isopropanol. After sonicating for 30 min, several drops of the resulting slurry were pipetted onto 3 mm holey carbon on Cu grids. Once dry, the grids were inserted into nontilt holders and loaded into a JEOL 4000EX II (line-to-line resolution = 0.14 nm; point-to-point resolution = 0.17 nm). Only regions overhanging holes in the carbon grid were used. The micrographs were in all cases taken at magnifications of either 150,000x or 500,000x.

After scanning in the micrographs at 400 dpi using a Silverscan II scanner, the measuring tool function in Image 1.59 was used to determine the particle diameters. The distances have been referenced to those for the {111} or {400} planes of γ-Al_2O_3 ($a = 0.792$ nm, Ref. (71)) and cross-referenced with the {111} or {200} planes of Rh ($a = 0.381$ nm, Ref. (71)) examined at 500,000x and scanned in at 600 dpi. This degree of accuracy, when combined with the distribution of planes observed throughout the material, was sufficient to make phase and plane identifications but was insufficient to detect any change in lattice parameter between the surface and bulk of the supported phase. Scale markers placed on the micrographs are accurate to within 3%.

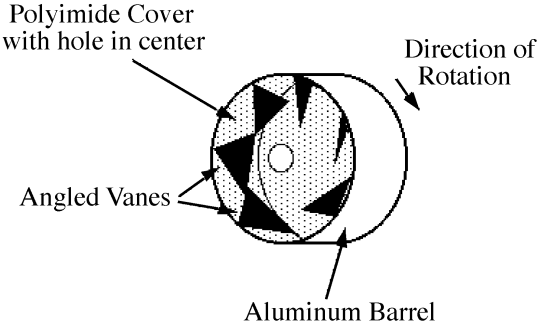

FIG. 2. Schematic of rotating basket target. Metal clusters impinge on alumina powder inside the basket. The basket is baffled and nearly full during deposition to improve homogeneity.

Catalytic HDS Testing

The laboratory scale liquid-phase continuous-flow HDS unit is shown schematically in Fig. 3. The reactor consisted of a thick-walled 0.375″ ID 316 SS tube, with the catalyst diluted with nonporous tabular alumina (LaRoche T-1061) sitting between plugs of quartz wool. Beneath the lower plug was a 0.125″ ID, 0.375″ OD deadman used to minimize volume between the reactor and the liquid receiver. The liquid test feed consisted of 1.0 wt% sulfur (as dibenzothiophene or DBT), dissolved in hexadecane and is representative of a middle distillate oil. All liquid-filled lines were heated to at least 50°C. Typical conditions for catalytic testing are summarized in Table 2.

The liquid products (typically 60 g/h) were weighed to permit later determination of mass balance closure. A small

TABLE 2

HDS Pilot Plant Operating Conditions

Liquid velocity = 0.25–1.00 g/min.	Pressure = 400 psig (1 psi = 6895 N m^{-2})
Gas velocity = 700 cc/min.	Preheater temperature = 300–500°C
$H_2/H_2S/N_2 = 5/0/2$	Furnace temperature = 200–400°C
Catalyst loading = 0.5–1.0 g	Catalyst temperature = ~30°C less than furnace
Tabular alumina diluent = 2.5–3.0 g	Liquid feed = 1.0 wt% S as dibenzothiophene
Liquid hourly space velocity = 5–40	(DBT) in normal hexadecane

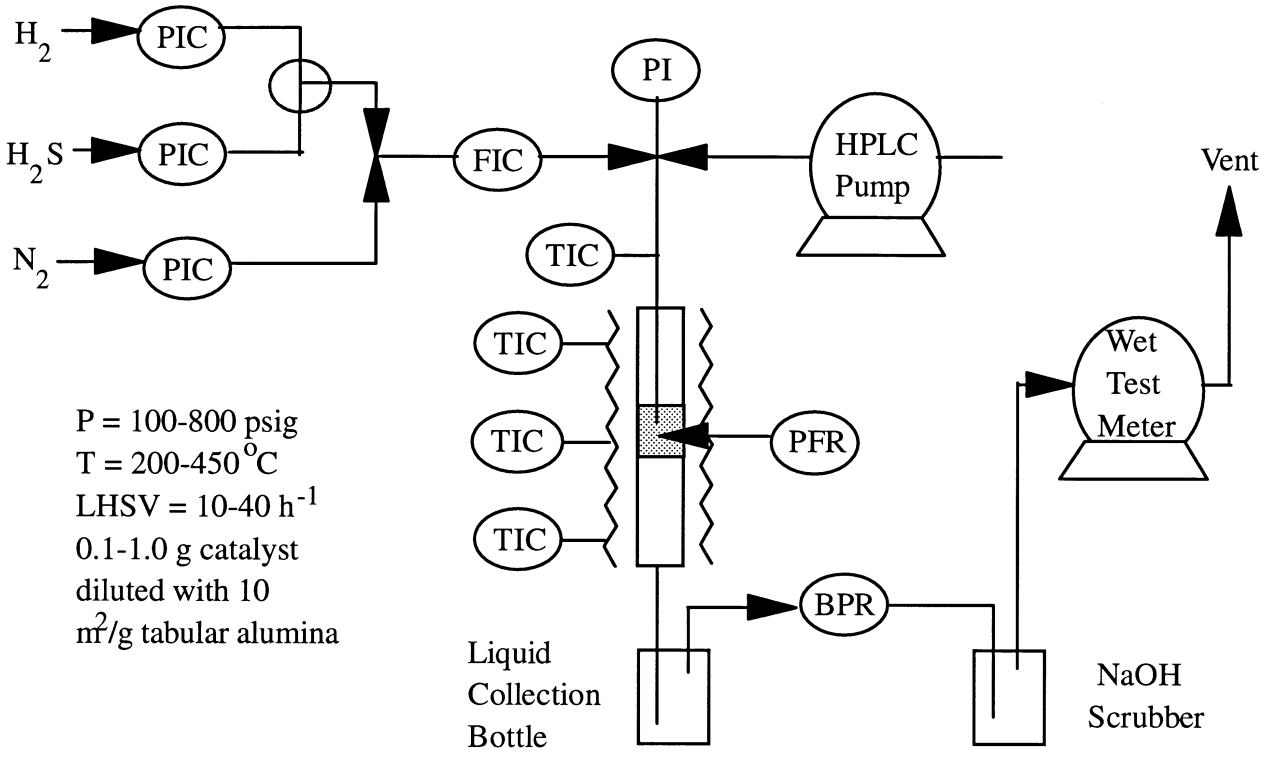

FIG. 3. Schematic of pilot plant hydrodesulfurization (HDS) catalyst testing unit.

aliquot (∼1 g) and a vial (∼20 g) of product was saved for later analysis. From the small aliquot, 100 mg of product was diluted to 10 ml with hexane, of which 30 μl was diluted further with hexane to 1.00 ml for gas chromatograph–mass spectrometric (GC–MS) analysis. The diluted products were separated using a DB5-MS column and analyzed using an HP 5890 GC–MS Series II Plus. Random errors associated with GC–MS concentration measurements were less than 5%, and the reproducibility of conversion measurements was ±15% of the reported values. Biphenyl yield has been defined as the number of moles of biphenyl product divided by the initial number of moles of dibenzothiophene. Selectivity has been defined as the percentage of biphenyl (the selective HDS product from dibenzothiophene) divided by the percentage of dibenzothiophene converted.

For comparison purposes, commercially available oxidized Co–Mo (Crosfield 465) and Ni–Mo (Crosfield 504), as well as 1 and 10% RhS_x/Al_2O_3 catalysts prepared here, were also tested for HDS activity. The RhS_x/Al_2O_3 (1 and 10% wt% Rh metal) catalysts were prepared from the incipient wetness impregnation of $RhCl_3 \cdot 3H_2O$ (99%, Alfa) into calcined LaRoche V–GL boehmite, followed by a second calcination at 600°C for 1 h in 1% O_2/He. The Crosfield 465, Crosfield 504, and 1 and 10% RhS_x/Al_2O_3 reference catalysts were first calcined at 600°C for 1 h in 1% O_2/He, cooled to room temperature under N_2, and stored in a N_2-purged glovebox for later use. The pretreatment schedule for both the Rh metal cluster-derived catalysts and the reference catalysts consisted of loading into the HDS reactor under N_2, purging in N_2 at 20°C for 30 min at 1000 cm^3/min., drying in N_2 at 150°C for 60 min and at 400°C for 60 min, and finally sulfiding in a 5% H_2S/H_2 mixture at 400°C for 2 h prior to use.

Temperature-Programmed Reduction

The hydrodesulfurization activities of a wide range of transition metal sulfides correlate with the ease of reduction of surface-bound sulfur (72). One way to determine the reducibility of a material is to heat the material at a fixed heating rate in the presence of H_2 and monitor the off-gases using either a thermal conductivity detector (used here) or a mass spectrometer. Such an experiment is hereafter referred to as temperature-programmed reduction.

Approximately 0.10 g of spent catalyst was placed into a 0.25″ ID stainless steel U-tube in between plugs of quartz wool and attached to an Altamira AMI-1 dynamic chemisorption apparatus. The pretreatment protocol consisted of purging in Ar at 35°C for 1 h, drying in Ar at 150°C for 1 h, heating in Ar to 500°C for 1 h, cooling in Ar to 450°C, reducing in H_2 at 450°C for 1 h, purging in Ar at 500°C, and cooling to 35°C in Ar. The temperature-programmed reduction (TPR) experiments for each catalyst consisted of

H_2 chemisorption at 35°C and 60 sccm for 1 h, followed by TPR at 10°C/min.

RESULTS

Mass Spectrometry of Gas Phase Clusters

Figure 4 displays the distributions of gas phase metal clusters used for the synthesis of the materials listed in Table 1. The mean size of the clusters used to generate the SR-1 material was extremely small (~35 atoms), whereas for the SR-3 material, the clusters were far larger (~200 atoms). Although there were several variables that were different between these runs, the reason most likely responsible for the larger clusters used to generate the SR-3 material was the use of the longer channel length between the metal target and exit nozzle. The key to generating small clusters was keeping the channel length short. Varying the temperature between cryogenic (SR-5) and room (SR-1) temperature had little, if any, effect on cluster size. The addition of O_2 (SR-4) or C_2H_4 (SR-6) reagent gas downstream of the cluster source did not significantly influence cluster size either. However, mass spectrometry of the clusters generated in the SR-4 and SR-6 runs indicated the presence of one oxygen (or carbon) atom per surface Rh atom, respectively.

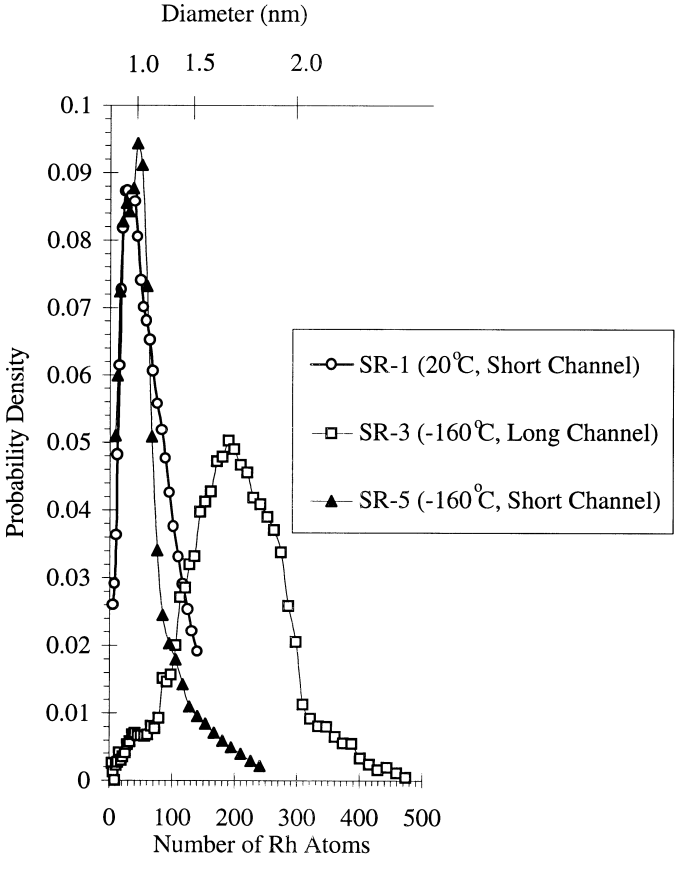

FIG. 4. Size distribution of Rh_n clusters for (○) SR-1, (□) SR-3, and (▲) SR-5 materials generated during metal cluster deposition.

Nonmetal incorporation into the clusters downstream of the Rh target was kinetically limited.

The cluster size distributions were fitted using the log-normal distribution (Eq. [1]) using the commercially available program PeakFit (Jandel Scientific)

$$f_{LN}(x) = \frac{1}{(2\pi)^{0.5}\ln(\sigma)} \exp\left(\frac{-[\ln(x/\bar{x})]^2}{2\ln^2(\sigma)}\right), \qquad [1]$$

where x is a given diameter, $f_{LN}(x)$ is the log-distributed probability density function, $\bar{x}$ is the log-mean diameter, and σ is the geometric standard deviation (73). Using this definition, one can show that the geometric standard deviation is equal to the diameter corresponding to a cumulative probability of 0.8413 divided by the log-mean diameter. Granqvist and Buhrman (73) have shown that Eq. [1] can be derived from particle coalescence theory, which is valid for all but the narrowest particle size distributions ($\sigma < 1.2$). For clusters or particles which grow via Ostwald ripening, the log-normal distribution has no theoretical justification. Nevertheless, Granqvist and Buhrman (73) have shown that distributions of clusters or particles grown by Ostwald ripening can be empirically fit to a good approximation with a log-normal distribution. We have chosen to fit both the vapor phase metal cluster sizes and alumina-supported metal particle sizes with the log-normal distribution so as to emphasize differences in the breadths of the respective particle size distributions. The mass spectral data show that the metal cluster size distributions are narrow ($\sigma < 1.2$), implying an Ostwald ripening growth mechanism.

Transmission Electron Microscopy

Particle size distributions were constructed by grouping the data into logarithmically evenly spaced bins ranging from 0.17 to 100 nm and then fit with one or two log-normal distributions as defined by Eq. [1]. The use of two log-normal distributions to describe the data was avoided except when absolutely necessary. The log means, geometric standard deviations, area percentages (for materials requiring two log-normal contributions), and numbers of particles counted are summarized in Table 3. The errors reported in Table 3 are standard deviations in the curve fit approximations to a given parameter and should not be confused with the actual errors in the particle size measurements. Wanke *et al.* (74) have shown that the sensitivity of particle size to defocus causes the reliability of size measurements for particles less than 2.5 nm (for 100 kV microscopes) to be unreliable. For 400 kV transmission electron microscopes such as the JEOL 4000EX II used in this work, size measurements for subnanometer particles must likewise be treated with caution, especially when one is dealing with a supported material. To ensure that the particle size data was as meaningful as possible, we took the following precautions:

TABLE 3

TEM Particle Sizes

Material	Log mean(s) (nm)	G.S.D.(s)[a]	Area %	Number of particles
SR-1	1.89 ± 0.04	1.43 ± 0.02	64	228
	6.8 ± 0.7	1.32 ± 0.10	36	
SR-1s	2.3 ± 0.3	1.37 ± 0.11	19	173
	7.3 ± 0.4	1.32 ± 0.05	81	
SR-3	2.01 ± 0.05	1.85 ± 0.02	100	460
SR-3s	2.0 ± 0.4	1.47 ± 0.15	18	293
	5.4 ± 0.3	1.35 ± 0.04	82	
SR-4	0.44 ± 0.03	1.26 ± 0.07	3	593
	1.93 ± 0.05	1.59 ± 0.03	97	
SR-5	0.52 ± 0.04	1.29 ± 0.09	5	430
	1.85 ± 0.10	1.67 ± 0.06	95	
SR-6	0.53 ± 0.02	1.19 ± 0.03	3	1048
	1.99 ± 0.04	1.66 ± 0.02	97	
SR-7	7.8 ± 0.7	1.34 ± 0.06	100	249
SR-7s	9.1 ± 1.0	1.33 ± 0.06	100	186
SR-8	0.48 ± 0.04	1.29 ± 0.08	4	632
	3.0 ± 0.2	1.47 ± 0.05	96	

Note. Reported errors are standard deviations of the curve fit approximations to a given parameter.

[a] G.S.D. = Geometric Standard Deviation = dimensionless measure of the breadth of the particle size distribution which can be determined by dividing the diameter corresponding to 84.13% probability by the log-mean diameter.

(1) In all cases, more than 100 particles were examined for each sample (Table 3). (2) Only Rh particles near the edges of the alumina particles were counted. (3) Histograms of the particle size distribution data shown later in this section include 95% prediction intervals, meaning that 95% of the points used to construct the curve fit approximations to the histograms must lie between the dashed lines. While we agree with Wanke *et al.* (73) that the reliability of an individual particle size measurement is questionable, our counting statistics do reliably allow us to determine whether or not a peak in the particle size distribution composed of subnanometer particles is real or not. For example, in Fig. 10, the small particle peak for SR-5 is clearly real, whereas a similar peak for SR-1 is not justified. In addition, the lack of scattering in the data contained in Figs. 10–12 provides strong evidence that reliable subnanometer particle size distribution information can be obtained when the aforementioned precautions are applied. However, the inherent uncertainty of individual particle size measurements does manifest itself by making the particle size distribution broader than it would otherwise be.

For convenience, we have included Eq. [2] to describe the relationship between Rh particle diameter (in nm) and the number of Rh atoms, where molecular weight is in g/mol and density in g/cm^3:

$$d(\text{nm}) = (\text{No. of atoms}) * \left[\frac{10^{21} * (\text{MW})}{(\rho)(N_{\text{AV}})^{1/3}}\right]. \qquad [2]$$

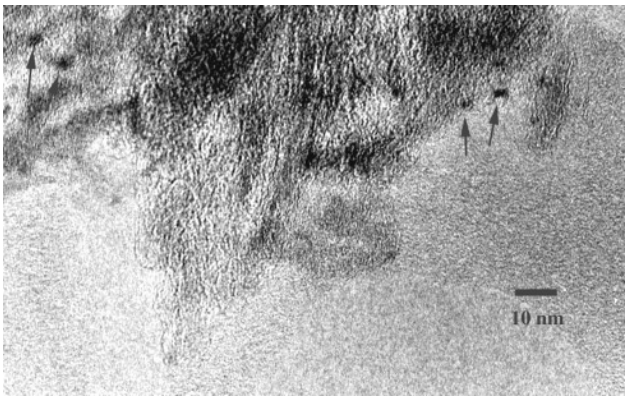

FIG. 5. TEM micrograph of SR-1.

Equation [2] assumes that the particles were spherical and of face-centered cubic structure. The micrographs confirmed that these were reasonable assumptions.

Representative microscope regions from each of the Rh-containing materials are shown in Figs. 5–9. The Rh particle size distribution of SR-1 was distinctly bimodal. Most of the particles in SR-1 were roughly 2 nm in size, but a significant minority of the particles was substantially larger (4–10 nm). The size distribution of the Rh particles in the SR-3 material was more uniform and once again about 2 nm in size. Most of the particles in the SR-4 material were also 2 nm in size, but there was also a statistically significant group of particles which were 0.3–0.6 nm.

The lattice fringe images (e.g., Fig. 7) of some of the larger particles in the materials prepared without reagent gas or exposure to sulfiding/HDS clearly indicated that the bulk structure of materials was face-centered cubic metallic rhodium. Transmission electron microscopy allowed us to say that the small amount of oxygen added in the SR-4 run was clearly insufficient to transform the Rh metal particles into a stoichiometric oxide. However, the insertion

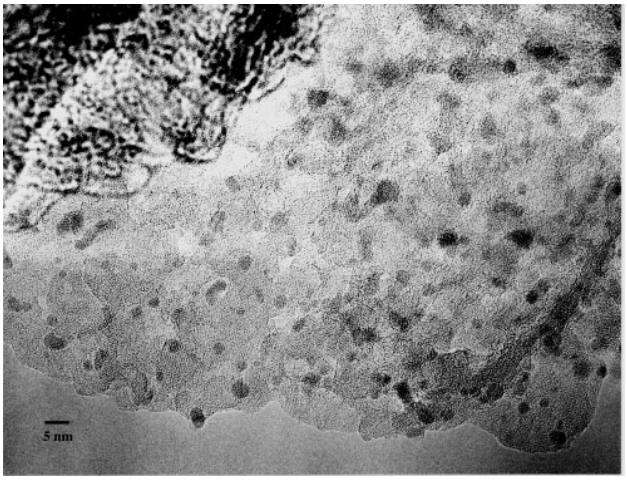

FIG. 6. TEM micrograph of SR-3.

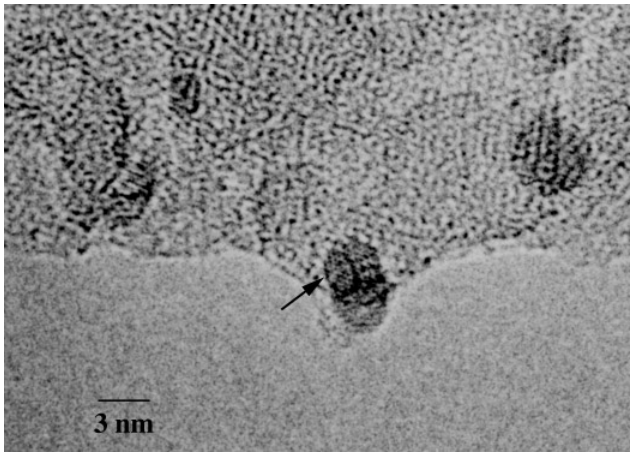

FIG. 7. Enlargement of Fig. 6 (SR-3) to show Rh face-centered cubic structure.

of carbon atoms into a Rh metal lattice during the SR-6 run would not sufficiently perturb the lattice framework for TEM to conclusively distinguish between Rh metal and Rh carbide phases.

Sulfiding and use as an HDS catalyst caused most of the particles in the SR-3s material to aggregate. None of the particles we examined from any of the sulfided materials (Fig. 8) were crystalline. Energy dispersive spectroscopy on the same grid of particles (using a JEM 100cx microscope) revealed that the S/Rh ratio was 1.4 ± 0.2, which suggests that the sulfiding was a bulk sulfiding to Rh_2S_3.

The particle size distribution data (points), the computer fit of the data (solid line), and the 95% prediction intervals (dashed lines) are shown for all the materials synthesized

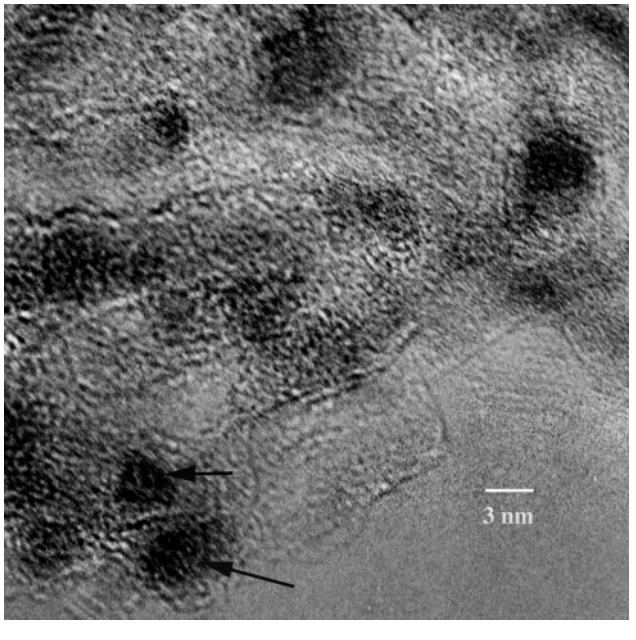

FIG. 8. TEM micrograph of SR-3s.

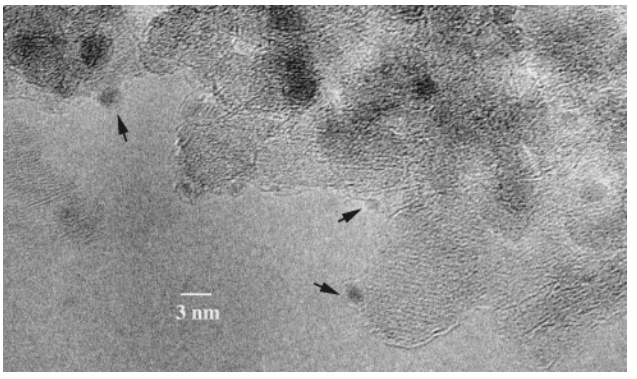

FIG. 9. TEM micrograph of SR-4.

in Figs. 10–12. This 95% prediction interval defines the confidence interval for an individual curve fit. The abscissa of these histograms has been scaled logarithmically to make the particle size distributions appear Gaussian. By comparing the particle size distributions for SR-1 (20°C) and SR-5 (−160°C), one can see that cryogenic cooling did help to limit metal aggregation (Fig. 10). However, by comparing the results of SR-3 and SR-5, one can see that despite the large difference in cluster sizes for these runs, the particle size distributions were nearly independent of channel

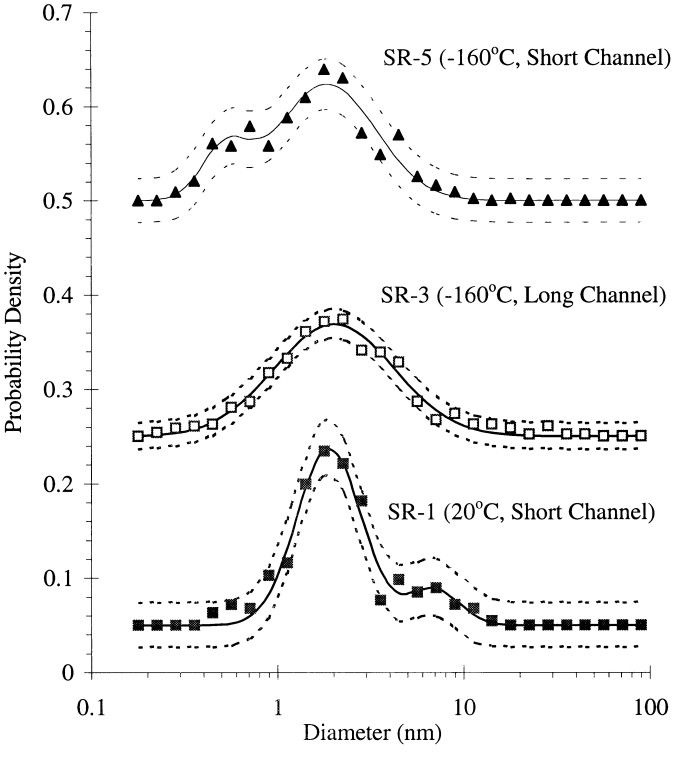

FIG. 10. The TEM particle size distributions of (■) SR-1, (□) SR-3, and (▲) SR-5 illustrate the attempts to synthesize subnanometer Rh particles. The vertical axis is probability density on a linear scale, and the horizontal axis is particle diameter on a logarithmic scale. Solid and dashed curves indicate the data fits and 95% prediction intervals, respectively.

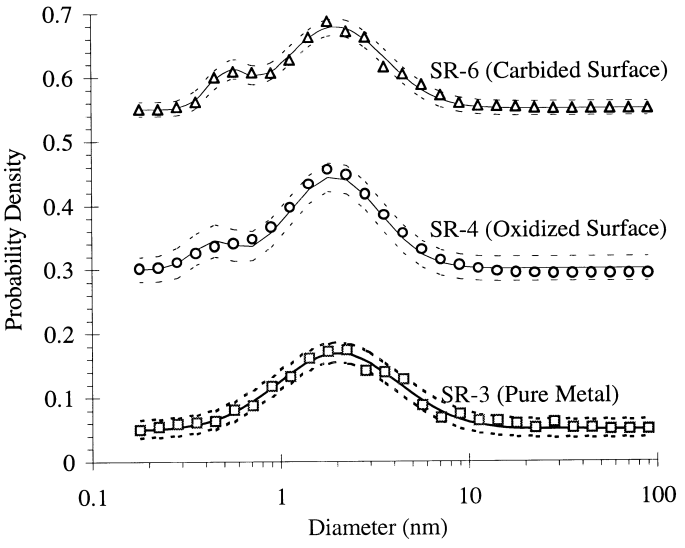

FIG. 11. The TEM particle size distributions of (□) SR-3, (○) SR-4, and (△) SR-6 illustrate the effect of reagent gas on the aggregation of Rh particles on the alumina surface. The vertical axis is probability density on a linear scale, and the horizontal axis is particle diameter on a logarithmic scale. Solid and dashed curves indicate the data fits and 95% prediction intervals, respectively.

length (Fig. 10). Adding either oxygen or ethylene downstream of the Rh target had little effect on particle size (Fig. 11). No face-centered cubic metal could be observed for the sulfided materials. The sulfiding caused a marked increase in particle size (Fig. 12).

The particle size distributions frequently consisted of a small, narrow peak centered at 0.5 nm and a much broader peak centered at 1.8–3.0 nm. These results suggest that only a few (3–5%) of the particles were derived from subnanometer clusters which did not aggregate on the alumina surface. The breadth of the peaks centered at 1.8–3.0 nm ($\sigma > 1.2$) were evidence that the larger particles were derived from aggregation of smaller clusters on the alumina surface.

HDS Activity Results

The SR-1, SR-3, and SR-7 materials were sulfided and then tested for the desulfurization of 1.0 wt% dibenzothiophene (DBT) in hexadecane, after which they were referred to as SR-1s, SR-3s, and SR-7s, respectively. Under all conditions tested, the HDS activities leveled off after 2 h on stream but were mass transfer limited, especially below 350°C. These mass transport limitations were controlled by the degree of aggregation of the oil and were catalyst-independent. At space velocities typical of those used in industrial hydrotreating units, we have observed similar transport limitations for a wide variety of sulfide catalysts and will describe these results in an upcoming paper (75).

The activities and selectivities were superior to a conventionally-prepared RhS_x/Al_2O_3 catalysts and commercial alumina-supported Co–Mo and Ni–Mo sulfides on a per gram of metal basis (Table 4). However, on a per gram of catalyst basis, the activities for the vapor-deposited materials were slightly less than those for the commercial catalysts (Table 5).

The SR-1s material synthesized by metal cluster deposition showed a moderate activity even at 250°C (Table 5). More importantly, the SR-1s catalyst was extremely selective to biphenyl, indicative of excellent hydrogen economy. In fact, at 250°C, biphenyl was the only product observed. It was hoped that by increasing the Rh loading that the activity of materials generated by metal cluster deposition would be equal or superior to commercial, sulfided Co–Mo and Ni–Mo catalysts. Unfortunately, not only was the activity per gram of catalyst of the SR-3s material even lower than the SR-1s material, but the selectivity to biphenyl was poorer as well. In order to assess whether a particle size effect might explain the relatively poor catalytic properties of SR-3s, cluster deposition parameters were chosen to generate a Rh/Al_2O_3 SR-7 material with much larger Rh particles. The large particle-containing SR-7 material, after sulfiding, was found to be both very active and highly selective to biphenyl.

Temperature-Programmed Reduction

Temperature-programmed reduction spectra for the sulfided Rh-containing SR-1s and SR-3s materials, as well as

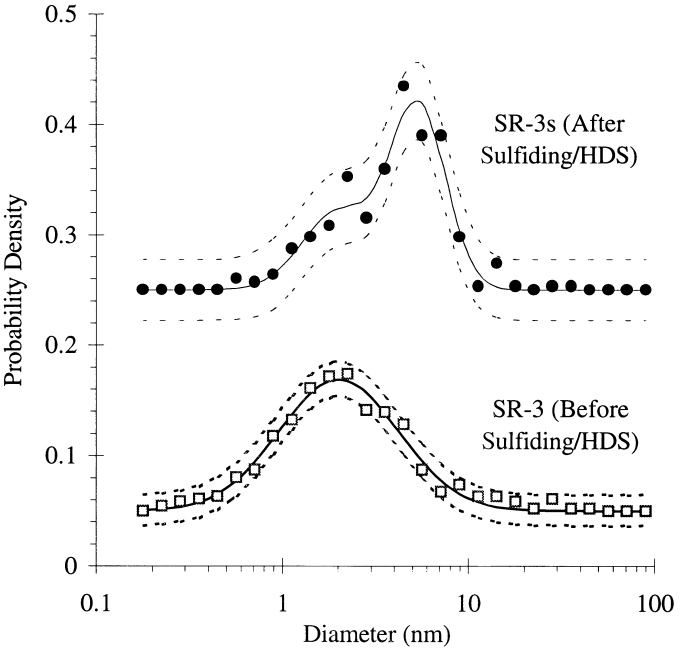

FIG. 12. The TEM particle size distributions of (□) SR-3 and (●) SR-3s illustrate the effect of sulfiding on particle aggregation. The vertical axis is probability density on a linear scale, and the horizontal axis is particle diameter on a logarithmic scale. Solid and dashed curves indicate the data fits and 95% prediction intervals, respectively.

TABLE 4

HDS Activities

Catalyst	HDS activity (Biphenyl selectivity) g DBT converted/ g metal–h (% biphenyl in product) 400°C	350°C	300°C	250°C
SR-1s		30.0 (90)		<5.0 (100)
SR-3s	8.8 (50)	4.0 (23)	<1.0 (40)	
SR-7s	18.0 (80)	12.0 (85)	3.6 (88)	1.0 (90)
1% RhS_x/Al_2O_3	2.0 (55)	0.80 (52)		
10% RhS_x/Al_2O_3	0.86 (64)	0.30 (66)		
Crosfield 465 (Co–Mo)	0.82 (80)	0.56 (91)	0.20 (85)	<0.05 (90)
Crosfield 504 (Ni–Mo)	0.98 (44)	0.58 (46)	0.27 (76)	0.10 (55)

Catalyst	HDS activity (Biphenyl selectivity) g DBT converted/ g surf. Rh[a]–h (% biphenyl in product) 400°C	350°C	300°C	250°C
SR-1s		86 (90)		<14 (100)
SR-3s	18 (50)	8 (23)	<2 (40)	
SR-7s	140 (80)	94 (85)	28 (88)	<8 (90)

[a] Surface Rh as measured before sulfiding by H_2 chemisorption at −78°C.

those for the Crosfield 465 and 504 catalysts, were quite similar to those reported by Mangnus *et al.* (72) for alumina-supported Rh and Co/Mo sulfides and, therefore, have not been shown. Mangnus *et al.* have correlated increasing thiophene HDS activity with ease of reduction of surface-bound sulfur in a wide variety of sulfide HDS catalysts (72). From Table 5, one can see that the temperatures of peak maxima for the reduction of surface-bound sulfur in our materials are consistent with those reported by Mangnus *et al.* (72).

TABLE 5

Reduction Temperature of the S_x Species and DBT Hydrodesulfurization Conversion

Catalyst	Temperature max S_x[a] (°C)	HDS Activity[b] (mg DBT converted/ g cat-h)
SR-1s	430	30
SR-3s	465	20
10% RhS_x/Al_2O_3	455	30
Rh/Al_2O_3 (Mangnus *et al.*)[c]	450	
Crosfield 465 (Co–Mo)	400	56
$Co–Mo/Al_2O_3$ (Mangnus *et al.*)[c]	400	
Crosfield 504 (Ni–Mo)	410	58

[a] Temperature corresponding to maximum rate of reduction of surface-bound sulfur.

[b] Dibenzothiophene (DBT) hydrodesulfurization activities measured at 350°C.

[c] Mangnus, P. J., Riezebos, A., van Langeveld, A. D., Moulijn, J. A., *J. Catal.* **151**, 178 (1995).

DISCUSSION

Nanoscale Particles

The Rh particle size determined by electron microscopy of the SR-1 sample was far larger than the 50-atom metal clusters generated by laser vaporization, indicating that despite their very low loading (0.1 wt% Rh), the Rh metal clusters deposited at room temperature had agglomerated on the alumina substrate. In an attempt to reduce or eliminate agglomeration, it was decided to reduce the temperature of the cluster source, minimizing both the clusters' internal energy and translational energy with which the clusters strike the target. The helium pressure was also reduced to keep constant the diffusional loss of metal atoms to the wall of the flow-tube. This makes the cluster growth rate roughly independent of temperature and leads to cluster size distributions that are also temperature independent. A comparison of the SR-1 and SR-5 distributions in Fig. 4 demonstrates that, under these conditions, comparable cluster sizes can be made at quite different temperatures. The effect of reduced temperature on the clusters' translational energy per metal atom is shown in Fig. 13. The translational energy of a 35-atom cluster, for example, was reduced from 14.9 eV for SR-1 to 6.5 eV for SR-5 (1 eV = 1.602×10^{-19} J). Measurements of the clusters' internal energy are not available, although the clusters' internal temperature is expected to be roughly proportional to the source temperature.

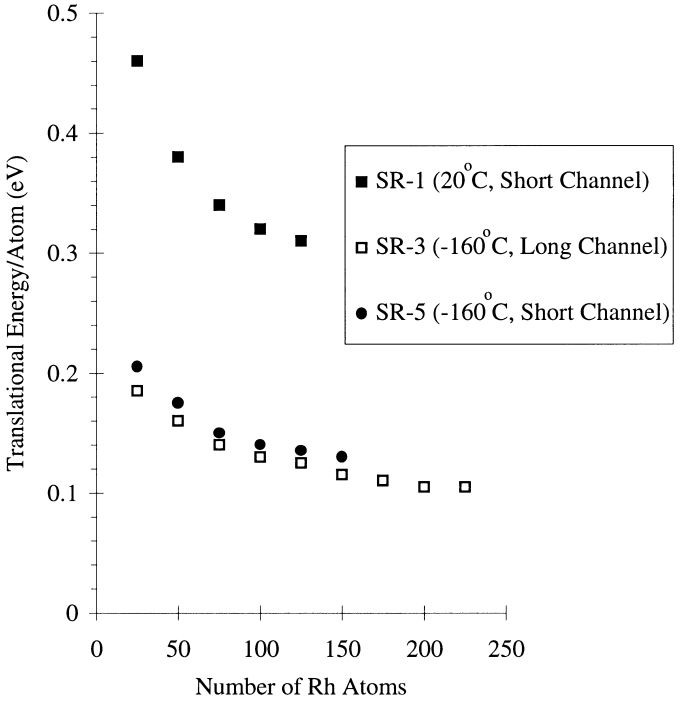

FIG. 13. Relationship between kinetic energy per Rh atom and Rh cluster size for (■) SR-1, (□) SR-3, and (●) SR-5.

Particle size distributions for SR-1 and SR-5 as measured by electron microscopy were essentially the same, averaging about 2 nm, indicating that reducing the clusters' internal and translational energy has little or no effect on the resulting agglomeration. Since the loading (deposition time) in SR-5 was considerably greater than in SR-1, surface loading does not seem to affect the final size of the agglomerated clusters. This result suggests that, once clusters reach a size of about 2 nm, they become immobile on the surface.

Increasing the channel length in the cluster source at constant source temperature and pressure had a dramatic effect on the gas phase cluster size distribution. SR-3 and SR-5 had the same temperature and pressure, but the longer channel length for SR-3 increased the average cluster size from 35 atoms to 200 atoms (roughly 2 nm in size). The electron microscopy analysis indicated a distribution centered around 2 nm for SR-3, again suggesting that 2 nm particles do not agglomerate on the surface, in agreement with the above conclusion.

Effect of Reactant Gas

Given that we were unable to stabilize subnanometer neutral Rh particles, we then tried to generate partly oxidized or carburized Rh clusters. The goal of these experiments was to determine whether or not deposition of a Rh-containing species in a nonzero oxidation state would prevent migration of subnanometer Rh-containing particles across the alumina surface, with the hope that these particles could be reduced to metallic Rh at a later time (e.g., prior to catalysis).

The effect of adding O_2 (SR-4) and C_2H_4 (SR-6) as a reagent gas was small (Fig. 11). Most of the particles were still near 2 nm in diameter. In addition, a small but statistically significant shoulder was present at 0.3–0.6 nm for the materials prepared using reagent gases. These shoulders were also observed in the mass spectrum for the SR-3 material. Based on a comparison of the mass spectra of the Rh clusters and the diameters of the alumina-supported Rh particles, it appeared that the presence of O_2 and C_2H_4 helped stabilize some, but clearly not many, of the smallest clusters deposited on the alumina support. For the most part, however, the addition of reagent gases following thermalization of the Rh clusters did little to decrease the average diameter of the supported Rh particles.

By adding O_2 upstream of the metal target, we grew RhO_x clusters in our final experiment (SR-8). Electron diffraction on some of the largest of the alumina-supported SR-8 particles were consistent with Rh_2O_3. However, these Rh_2O_3 particles in SR-8 were larger (3.0 nm) than in any of the seven previous runs. It was hoped that an oxidized Rh cluster would anchor itself on the alumina support more strongly and thus prevent aggregation of the precious metal. However, the Rh oxide clusters grew so rapidly prior to deposition that there was no chance of generating subnanometer Rh oxide particles by adding oxygen upstream of the Rh target. Rapid nucleation and growth was also recently reported for neutral Mn oxide clusters (76).

Particle growth for all Rh clusters, regardless of oxidation or carburization treatments, continued until the particles reached a critical size of about 1.5–2.0 nm. Not coincidentally, this diameter corresponded to the point at which the translational energy per atom of the incoming Rh clusters reached a plateau (Fig. 13). At smaller diameters, there is still a driving force in translational energy for aggregation in the vapor phase. This driving force appears to extend to the solid phase (Al_2O_3-supported Rh).

Conventional methods for the preparation of supported metals involve either impregnation or spray-drying of an aqueous metal salt precursor into the support. The oxidation state of the metal in the metal salt is always positive. In contrast, the experiments discussed in this section involved the deposition of neutral (metallic) clusters onto an alumina support. We then asked ourselves what differences we would expect if we vapor deposited Rh^{+3} clusters onto an alumina support. Since the helium carrier gas supplies much of the translational energy to the clusters, the primary difference between the translational energy per atom (or ion) would be due to the increased collisional cross section for the ionic species. Our calculations suggest that the difference in collisional cross section is only significant for clusters less than 50 atoms large, and, thus, we would expect aggregation of ionic Rh clusters to 1.5–2.0 nm just as we have observed for the neutral metal clusters.

Effect of Sulfiding/HDS

The combined effects of sulfiding and use of the SR-3 material as an HDS catalyst had a dramatic effect on the Rh particle size distribution. From Fig. 12, by comparing the particle size distributions of SR-3 and SR-3s, one can see that only a small fraction of the starting material remained at 2-nm diameter and that most of the sulfided Rh had agglomerated to form larger particles (3–9 nm).

Particle Size Dependence on HDS Catalytic Properties

A trend between ease of reduction and HDS activity has already been reported (72). We observed the same trend for both the Rh-containing materials and sulfided commercial catalysts (Table 5). The low-loaded SR-1s material, composed of both 2- and 7-nm spherical particles, was somewhat more active and far more selective than the much higher-loaded SR-3s material, which was comprised of a mixture of 2- and 5-nm particles. The SR-7s material, composed of 9-nm particles, was quite active and selective.

The simplest interpretation of these results is that the smaller particles were less effective for hydrodesulfurization of dibenzothiophene than the larger particles. In fact, a concurrent study of dibenzothiophene (DBT) hydrodesulfurization over supported nitrides and carbides has

suggested that small particles are less active for HDS than larger particles (75). These results prompt the question of how the adsorption energetics of DBT onto a spherical surface vary as a function of particle size (radius of curvature) and will be the subject of ongoing work.

Such particle size dependences on HDS activity have not been reported for Mo-based sulfide catalysts. Even though the Mo sulfide domains can be very highly dispersed, the raft-like structure of MoS_2 is typically a nearly flat surface and always conforms to the morphology of the underlying support. However, recent work by Datye *et al.* (77) on MoS_2/TiO_2–SiO_2 suggests that pyridine hydrodenitrogenation (HDN) is faster on MoS_2 domains with radii of curvature ranging from 2–5 nm. The HDN selectivities in Datye's experiments indicated that the direct denitrogenation of the C=N bond was quite slow compared to the pathway initiated by ring hydrogenation (HYD), which implies that the pyridine is π-bound to the Mo sulfide surface. Both the structures of organometallic clusters with dibenzothiophene (DBT) ligands (78–82) and the HDS selectivity results for Mo/Al_2O_3 (83–85), Co–Mo/Al_2O_3 (86), Ru/Al_2O_3 (87–88), and Rh/Al_2O_3 sulfide catalysts (75) indicate that dibenzothiophene binds through the sulfur atom to these catalysts.

CONCLUSIONS

A series of highly dispersed Rh-based materials have been prepared by deposition of laser-generated clusters onto an industrial-grade alumina. While the diameter of the growing rhodium clusters could be kept at or below 1 nm, the average diameter of the resulting supported Rh particles was always at least 1.5 nm. The reaction of the clusters with either O_2 or C_2H_4 prior to deposition failed to prevent Rh aggregation. In all cases, lattice fringe images of the Rh-containing particles suggested that the bulk structure was metallic Rh, even when O_2 or C_2H_4 was added downstream of the Rh target. Surprisingly, Rh oxide clusters aggregated to form larger particles than Rh metal clusters under otherwise identical conditions.

Most of the Rh-containing particles further aggregated during either sulfiding or HDS testing. Nevertheless, the resulting Rh sulfides were comparable in activity to sulfided, commercial Co(Ni)–Mo catalysts on a per gram of catalyst basis and far superior on a per gram of metal basis. In addition, the vapor-deposited Rh sulfide catalysts were more hydrogen-efficient at low loadings. The most active and selective materials were composed of larger Rh sulfide particles.

ACKNOWLEDGMENTS

This work was performed under the auspices of the U.S. Department of Energy, Office of Basic Energy Sciences, Division of Chemical Sciences under contract number W-31-109-ENG-38 (cluster generation by G. C. N., E. K. P., and S. J. R.) and the Office of Fossil Energy—Bartlesville. This work made use of TEM facilities at the Electron Microscopy Center for Materials Research at Argonne National Laboratory. We thank Heinz Robota of Allied Signal for construction of the cylindrical collection basket.

REFERENCES

1. Parks, E. K., Winter, B. J., Klots, T. D., and Riley, S. J., *J. Chem. Phys.* **94**, 1882 (1991).
2. Klots, T. D., Winter, B. J., Parks, E. K., and Riley, S. J., *J. Chem. Phys.* **95**, 8919 (1991).
3. Winter, B. J., Klots, T. D., Parks, E. K., and Riley, S. J., *Z. Phys. D* **19**, 375 (1991).
4. Winter, B. J., Klots, T. D., Parks, E. K., and Riley, S. J., *Z. Phys. D* **19**, 381 (1991).
5. Yamada, Y., and Castleman, A. W., *J. Chem. Phys.* **97**, 4543 (1992).
6. Rohlfing, E. A., Cox, D. M., Kaldor, A., and Johnson, K. H., *J. Phys. Chem.* **88**, 6227 (1984).
7. Bondybey, V. E., English, J. H., and Schwartz, G. P., *J. Chem. Phys.* **78**, 11 (1983).
8. Gole, J. L., Bondybey, V. E., and English, J. H., *J. Phys. Chem.* **86**, 2560 (1982).
9. *Chem. Eng. News* **63**(3), 51 (1991).
10. LaiHing, K., Cheng, P. Y., and Duncan, M. A., *J. Phys. Chem.* **91**, 6521 (1987).
11. Pastor, G. M., Bennemann, K. H., and Dorantesdavila, J., *Chem. Phys. Lett.* **148**, 459 (1988).
12. Freiser, B. S., *Anal. Chim. Acta* **178**, 137 (1985).
13. Bowles, R. S., Andres, R. P., Otsuka, N., and Park, S. B., *J. Mol. Catal.* **20**, 279 (1983).
14. Mahoney, W., and Andres, R. P., *Mater. Sci. Eng. A* **204**, 160 (1995).
15. Chao, L. C., and Andres, R. P., *J. Colloid Interface Sci.* **165**, 290 (1994).
16. Schulze, W., Charle, K. P., Frank, F., and Tesche, B., *Ber. Bunsenges. Phys. Chem.* **88**, 263 (1984).
17. Schumacher, E., Kappes, M., Marti, K., Radi, P., and Schar, M., *Ber. Bunsenges. Phys. Chem.* **88**, 220 (1984).
18. Giorgio, S., and Urban, J., *Z. Phys. D* **12**, 115 (1989).
19. Faust, P., Brandstattner, M., and Ding, A., *Z. Phys. D* **21**, 285 (1991).
20. Sattler, K., *Z. Phys. D* **19**, 287 (1991).
21. Usui, H., Takagi, T., Tanaka, M., and Yamada, I., *Nucl. Instrum. Methods Phys. Res. B* **37**, 886 (1989).
22. Yang, S. N., and Lu, T. M., *Appl. Phys. Lett.* **48**, 1122 (1988).
23. Upton, T. H., *Phys. Rev. Lett.* **56**, 2168 (1986).
24. Kaldor, A., and Cox, D. M., *Pure Appl. Chem.* **62**, 79 (1991).
25. Bechthold, P. S., Parks, E. K., Weiller, B. H., Pobo, L. G., and Riley, S. J., *Z. Phys. Chem. Neue Folge* **169**, 101 (1990).
26. Riley, S. J., Parks, E. K., Pobo, L. G., and Wexler, S., *Ber. Bunsenges. Phys. Chem.* **88**, 287 (1984).
27. Riley, S. J., Parks, E. K., Nieman, G. C., Pobo, L. G., and Wexler, S., *J. Chem. Phys.* **80**, 1360 (1984).
28. Knickelbein, M. B., and Menezes, W. J. C., *J. Phys. Chem.* **96**, 6611 (1991).
29. Guo, B. C., Kerns, K. P., and Castleman, A. W., *J. Phys. Chem.* **96**, 6931 (1991).
30. Guo, B. C., Wei, S., Chen, Z., Kerns, K. P., Purnell, J., Buzza, S., and Castleman, A. W., *J. Chem. Phys.* **97**, 5243 (1992).
31. Brucat, P. J., Craycraft, M. J., Pettiette, C. L., Smalley, R. E., Yang, S., and Zheng, L. S., *J. Chem. Phys.* **85**, 4747 (1986).
32. Geusic, M. E., Smalley, R. E., O'Brien, S. C., and Morse, M. D., *Rev. Sci. Inst.* **56**, 2123 (1985).
33. Castleman, A. W., Harms, A. C., and Leuchtner, R. E., *Z. Phys. D* **19**, 343 (1991).

34. Nakajima, T., Kishi, T., Sone, Y., Nonose, S., and Kaya, K., *Z. Phys. D* **19**, 385 (1991).
35. Fayet, P., and Wõste, L., *Z. Phys. D* **3**, 177 (1986).
36. Knickelbein, M. B., *J. Chem. Phys.* **99**, 2377 (1993).
37. Rohlfing, E. A., Cox, D. M., Kaldor, A., and Johnson, K. H., *J. Chem. Phys.* **81**, 3846 (1984).
38. Rohlfing, E. A., Cox, D. M., and Kaldor, A., *J. Phys. Chem.* **88**, 4497 (1984).
39. Rohlfing, E. A., Cox, D. M., and Kaldor, A., *Chem. Phys. Lett.* **99**, 161 (1983).
40. Morse, M. D., and Smalley, R. E., *Ber. Bunsenges. Phys. Chem.* **88**, 228 (1984).
41. Hopkins, J. B., Langridge-Smith, P. R. R., Morse, M. D., and Smalley, R. E., *J. Chem. Phys.* **78**, 1627 (1983).
42. Powers, D. E., Dietz, T. G., Duncan, M. A., Geusic, M. E., Hansen, S. G., Hopkins, J. B., Langridge-Smith, P. P. R., Puiu, A. C., and Smalley, R. E., *J. Phys. Chem.* **86**, 2556 (1982).
43. Delacrataz, G., Fayet, P., and Wõste, L., *Ber. Bunsenges. Phys. Chem.* **88**, 284 (1984).
44. Pastor, G. M., Bennemann, K. H., and Dorantesdavila, J., *Chem. Phys. Lett.* **148**, 459 (1988).
45. Ozin, G. A., and Mitchell, S. A., *Angew. Chem.* **22**, 674 (1983).
46. Pellarin, M., Vialle, J. L., Lerme, J., Valadier, F., Baguenard, B., Blanc, J., and Broyer, M., *J. Phys. IV* **1**, 725 (1991).
47. Wucher, A., *Phys. Rev. B* **49**, 2012 (1994).
48. Zhao, J. J., Han, M., and Wang, G. H., *Phys. Rev. B* **48**, 15297 (1993).
49. Bucher, J. P., Douglass, D. C., Xia, P., Haynes, B., and Bloomfield, L. A., *Z. Phys. D* **19**, 251 (1991).
50. Louderback, J. G., Cox, A. J., Lising, L. J., Douglass, D. C., and Bloomfield, L. A., *Z. Phys. D* **26**, 301 (1993).
51. Billas, I. M. L., Chatelain, A., and deHeer, W. A., *Science* **265**, 1682 (1994).
52. Apsel, S. E., Emmert, J. W., Deng, J., and Bloomfield, L. A., *Phys. Rev. Lett.* **76**, 1441 (1996).
53. Dunlap, B. I., *Z. Phys. D* **19**, 255 (1991).
54. Bucher, J. P., Douglass, D. C., and Bloomfield, L. A., *Phys. Rev. Lett.* **66**, 3052 (1991).
55. Douglass, D. C., Cox, A. J., Bucher, J. P., and Bloomfield, L. A., *Phys. Rev. B Condens. Matter* **47**, 12874 (1993).
56. Cox, A. J., Louderback, J. G., and Bloomfield, L. A., *Phys. Rev. Lett.* **71**, 923 (1993).
57. Cox, A. J., Louderback, J. G., Apsel, S. E., and Bloomfield, L. A., *Phys. Rev. B Condens. Matter* **49**, 12295 (1994).
58. Dietz, T. G., Duncan, M. A., Powers, D. E., and Smalley, R. E., *J. Phys. Chem.* **74**, 6511 (1981).
59. Michalopoulos, D. L., Guesic, M. E., Hansen, S. G., Powers, D. E., and Smalley, R. E., *J. Phys. Chem.* **86**, 2556 (1982).
60. Bondybey, V. E., *J. Phys. Chem.* **86**, 3396 (1982).
61. Gole, J. L., Bondybey, V. E., and English, J. H., *J. Phys. Chem.* **86**, 2560 (1982).
62. Bondybey, V. E., and English, J. H., *J. Chem. Phys.* **76**, 2165 (1982).
63. Parks, E. K., Weiller, B. H., Bechthold, P. S., Hoffman, W. F., Nieman, G. C., Pobo, L. G., and Riley, S. J., *J. Chem. Phys.* **88**, 1622 (1988).
64. Parks, E. K., and Riley, S. J., *in* "The Chemical Physics of Atomic and Molecular Clusters" (G. Scoles, Ed.), Proc. S.I.F. Course CVII, pp. 761–777. Elsevier, Amsterdam, 1990.
65. Lifshitz, I.M., and Slyozhov, J., *J. Phys. Chem. Solids* **19**, 35 (1961).
66. Poppa, H., *Catal. Rev. Sci. Eng.* **35**, 359 (1993).
67. Usui, H., Takagi, T., Tanaka, M., and Yamada, I., *Nucl. Instrum. Methods Phys. Res. B* **37**, 886 (1989).
68. Giorgio, S., and Urban, J., *Z. Phys. D* **12**, 115 (1989).
69. Sattler, K., *Z. Phys. D* **19**, 287 (1991).
70. Yamada, I., Inakawa, H., and Takagi, K., *J. Appl. Phys.* **56**, 2746 (1984).
71. International Centre for Diffraction Data, Swarthmore, PA, 1993.
72. Mangnus, P. J., Riezebos, A., van Langeveld, A. D., and Moulijn, J. A., *J. Catal.* **151**, 178 (1995).
73. Granqvist, C. G., and Buhrman, R. A., *J. Appl. Phys.* **47**, 2200 (1976).
74. Flynn, P. C., Wanke, S. E., and Turner, P. S., *J. Catal.* **33**, 178 (1995).
75. Brenner, J. R., Thiyagarajan, P., Ellis, L., Anderson, K. B., Tomczyk, N. A., Marshall, C. L., and Winans, R. E., in preparation.
76. Parks, E. K., Nieman, G. C., and Riley, S. J., *J. Chem. Phys.* **104**, 3531 (1996).
77. Datye, A. K., Srinivasan, S., Allard, L. F., Peden, C. H. F., Brenner, J. R., and Thompson, L. T., *J. Catal.* **158**, 205 (1996).
78. Sánchez-Delgado, R. A., *J. Mol. Catal.* **86**, 287 (1994).
79. Bianchini, C., Jiménez, M. V., Meli, A., Moneti, S., Vizza, F., Herrera, V., and Sánchez-Delgado, R. A., *Organometallics* **14**, 2342 (1995).
80. Bianchini, C., Casares, J. A., Jiménez, M. V., Meli, A., Moneti, S., Vizza, F., Herrera, V., and Sánchez-Delgado, R. A., *Organometallics* **14**, 4850 (1995).
81. Garcia, J. J., and Maitlis, P. M., *J. Am. Chem. Soc.* **115**, 12200 (1993).
82. Garcia, J. J., Mann, B. E., Adams, H., Bailey, N. A., and Maitlis, P. A., *J. Am. Chem. Soc.* **117**, 2179 (1995).
83. Daage, M., and Murray, H. H., *Prepr. Am. Chem. Soc. Div. Petr. Chem.* **38**, 660 (1993).
84. Daage, M., and Chianelli, R. R., *J. Catal.* **149**, 414 (1994).
85. Ishihara, A., Nomura, M., and Kabe, T., *Chem. Lett.* 589 (1993).
86. Isoda, T., Ma, X., and Mochida, I. *Prepr. Am. Chem. Soc. Div. Petr. Chem.* **39**, 584 (1994).
87. Ishihara, A., Nomura, M., and Kabe, T., *J. Catal.* **150**, 212 (1994).
88. Ishihara, A., Nomura, M., and Kabe, T., *Chem. Lett.* 2285 (1992).